The Small Mars System

E. Fantino[a], M. Grassi[b], P. Pasolini[b], F. Causa[b], C. Molfese[c], R. Aurigemma[d], N. Cimminiello[d], D. de la Torre[a], P. Dell'Aversana[e], F. Esposito[c], L. Gramiccia[f], F. Paudice[b], F. Punzo[e], I. Roma[g], R. Savino[b], G. Zuppardi[b]

[a] *Space Studies Institute of Catalonia (IEEC), Barcelona (Spain)*
[b] *University of Naples "Federico II", Naples (Italy)*
[c] *INAF - Astronomical Observatory of Capodimonte, Naples (Italy)*
[d] *Eurosoft srl, Naples (Italy)*
[e] *ALI S.c.a.r.l., Naples (Italy)*
[f] *SRS E.D., Roma (Italy)*
[g] *ESA/ESTEC, Noordwijk (The Netherlands)*

Abstract

The Small Mars System is a proposed mission to Mars. Funded by the European Space Agency, the project has successfully completed Phase 0. The contractor is ALI S.c.a.r.l., and the study team includes the University of Naples "Federico II", the Astronomical Observatory of Capodimonte and the Space Studies Institute of Catalonia. The objectives of the mission are both technological and scientific, and will be achieved by delivering a small Mars lander carrying a dust particle analyser and an aerial drone. The former shall perform *in situ* measurements of the size distribution and abundance of dust particles suspended in the Martian atmosphere, whereas the latter shall demonstrate low-altitude flight in the rarefied planetary environment. The mission-enabling technology is an innovative umbrella-like heat shield, known as IRENE, developed and patented by ALI. The mission is also a technological demonstration of the shield in the upper atmosphere of Mars. The core characteristics of SMS are the low cost (120 M€) and the small size (320 kg of wet mass at launch, 110 kg at landing), features which stand out with respect to previous Mars landers. To comply with them is extremely challenging at all levels, and sets strict requirements on the choice of the materials, the sizing of payloads and subsystems, their arrange-

*Corresponding author: elena.fantino@gmail.com (E. Fantino)

ment inside the spacecraft and the launcher's selection. In this contribution, the mission and system concept and design are illustrated and discussed. Special emphasis is given to the innovative features and to the challenges faced in the development of the work.

Keywords: Space missions, Planetary exploration, Mars landers

1. Introduction

The robotic exploration of Mars has yielded a dramatic increase in knowledge about the Martian system. Since 1976, the surface probing of Mars has been carried out with a series of landers: Viking 1 and 2 [1], Mars Pathfinder [2], the two Mars Exploration Rovers [3], Phoenix [4] and Mars Science Laboratory [5]. The majority of these missions belong to NASA's Mars Exploration Program whose goals are to determine whether life ever developed on Mars, to characterize the climate, to understand the geology, and eventually to prepare for the human exploration of the planet. As a complement, NASA's Discovery Program, started in 1992, focuses planetary science investigations by launching smaller missions using fewer resources and shorter development times. The Discovery Program includes Mars Pathfinder and the geophysical Mars lander InSight planned for 2018 [6].

Establishing if life ever existed on Mars is one of the outstanding scientific questions of our time. To address this important goal, the European Space Agency (ESA) has established the ExoMars programme to investigate the Martian environment and to demonstrate new technologies paving the way for a future Mars sample return mission in the 2020's. ExoMars comprises two missions: ExoMars 2016 has recently delivered the Trace Gas Orbiter [7], whereas the second mission features a rover and has a launch date in 2020 [8].

The Small Mars System (SMS) is being designed as a European technology demonstration and science mission in the category of small, low-cost landers. It was proposed by ALI S.c.a.r.l. to ESA with the aim of experimenting an innovative deployable heat shield (DHS), whose first version, known as IRENE

(Italian ReEntry NacellE, [9]), is conceived for terrestrial applications, such as returning payloads from the International Space Station. The mission objectives of SMS were later extended to include two payloads: a dust particle analyser (DPA) and an aerial drone (AD). The DHS, developed and patented by ALI, is a modular atmospheric entry shield. Its main characteristics are the umbrella-like opening mechanism and the innovative off-the-shelf ceramic material. The DHS is lightweight, hence suitable for a low-mass spacecraft. The DPA is a scientific instrument developed at the Astronomical Observatory of Capodimonte (INAF-AOC). Heritage of previous experiments (DREAMS, [10]; MEDUSA, [11]; GIADA, [12]), the DPA measures the concentration and size distribution of the dust grains present in the atmosphere, key elements in the study of the Martian climate and in the definition of the entry-descent-landing requirements of future exploration missions, including manned ones. The AD is being designed at the University of Naples "Federico II" and aims at demonstrating low-altitude flight in the rarefied atmosphere of the red planet. During flight, an imaging camera on board the AD shall take high-resolution pictures of the surface, thus enhancing the scientific return of the mission.

In its current configuration, SMS has a wet mass just above 300 kg, 110 kg constituting the mass of the lander. The cylindrical envelope of the spacecraft has a size of 2 m (diameter) $\times$ 3 m (height). Current estimates for the total mission cost are close to 120 M€ including launch and operations. Such a low value will be made possible, on the one hand, by relying on the heritage of previous missions, by implementing recently developed technology (e.g., the DHS), and by adopting commercial-off-the-shelf (COTS) hardware and lightweight materials, and by making a strong effort in terms of design optimization, synergy among the several subsystems and efficiency in mission planning, on the other. The short duration of the operations (eleven months of interplanetary transfer plus a few days of scientific activity on the surface) and the reduced mass and volume of the spacecraft (which comply with the performance characteristics of the Vega rocket, the European launcher for small payloads) further contribute to the cost reduction. The majority of past missions of the kind were much bigger

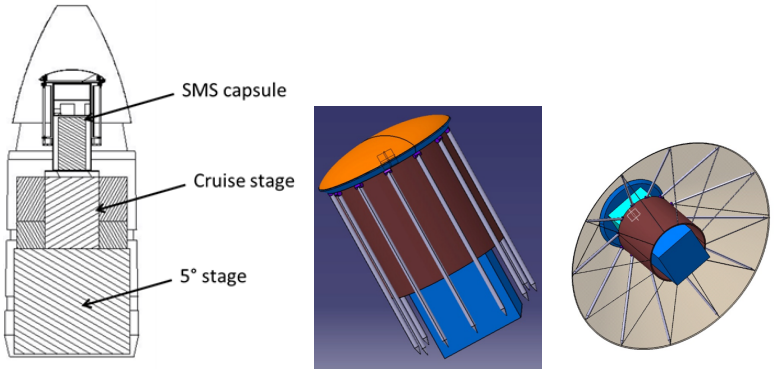

Figure 1: Left: SMS (Lander + DHS), CS and PM after assembly and packing in the payload fairing of Vega; Center and right: the Lander inside the DHS in folded and unfolded configuration, respectively.

in size and mass, and more expensive, the cheapest being Mars Pathfinder worth 265 M$ and the high-end being Mars Science Laboratory (2500 M$). These missions had a much wider scientific reach and engineering dimension, though. SMS aims at proving the technical viability of a Mars lander of smaller size and the possibility of retrieving scientific data of relevance to the international community. The Phase 0 of the project, conducted between November 2015 and May 2016, has proven the feasibility of SMS. All mission design elements have been addressed and developed at an appropriate level for this preliminary phase.

Section 2 illustrates the mission concept and time frame. Section 3 describes the two payloads. Section 4 deals with the selection of the launcher, the choice of the launch date, the definition of the launch profile, the design of the interplanetary trajectory and the approach to Mars. Section 5 contains a description of the entry, descent and landing (EDL) phase. This is followed by the illustration of the design of the DHS (Sect. 6). The subsystems design is outlined in Sect. 7. Conclusions are drawn in Sect. 8.

2. Mission concept and time frame

SMS has the twofold objective of demonstrating the effectiveness of a deployable thermal shielding technology for planetary entry and the capability of a small, low-cost system to deliver scientific and technological payloads to Mars. The spacecraft consists of three main parts, as shown in Fig. 1 (left) illustrating the launch setup in the payload fairing of a Vega rocket: the Lander stowed inside the DHS (in retracted configuration), the cruise stage (CS) and the propulsion module (PM). The PM shall act as an additional (fifth) stage at launch. Its presence is necessary because Vega does not achieve Earth escape. The PM will separate from the spacecraft after executing the injection into interplanetary trajectory, leaving a total mass of 304 kg (including propellant). The CS shall provide telecommunications, photovoltaic power and propulsion (see Sect. 7) during interplanetary transfer and will be jettisoned shortly before atmospheric entry, leaving a mass of 150 kg. The Lander contains the payloads (i.e., the AD and the DPA) and the avionics and has a mass of 110 kg at touch down, resulting from the release of the DHS and the parachute.

According to the baseline mission profile, SMS shall be placed on a direct transfer from Earth to Mars and shall enter Mars atmosphere from a direct hyperbolic trajectory. **Since no Mars orbit insertion is foreseen, SMS will not deliver an orbiter and shall rely on the availability of an existing one for telecommunications.** Upon entering the atmosphere, an umbrella-like mechanism will unfold the shield, stowed at launch and during the interplanetary cruise (see Fig. 1 center and right). In this way, the shield occupies little space in the payload fairing, a feature which allows the adoption of a small launcher. The descent phase will exploit the DHS and a subsonic parachute to reduce speed. Soft landing will be aided by a vented airbag stowed in the nose of the capsule. Once on ground, the cover of the lander will unfold (Figs. 2 and 3) exposing the payloads and the antenna. Operations on the surface of Mars should last from a few days to a few weeks.

Thermal and safety considerations affect the choice of the landing site and

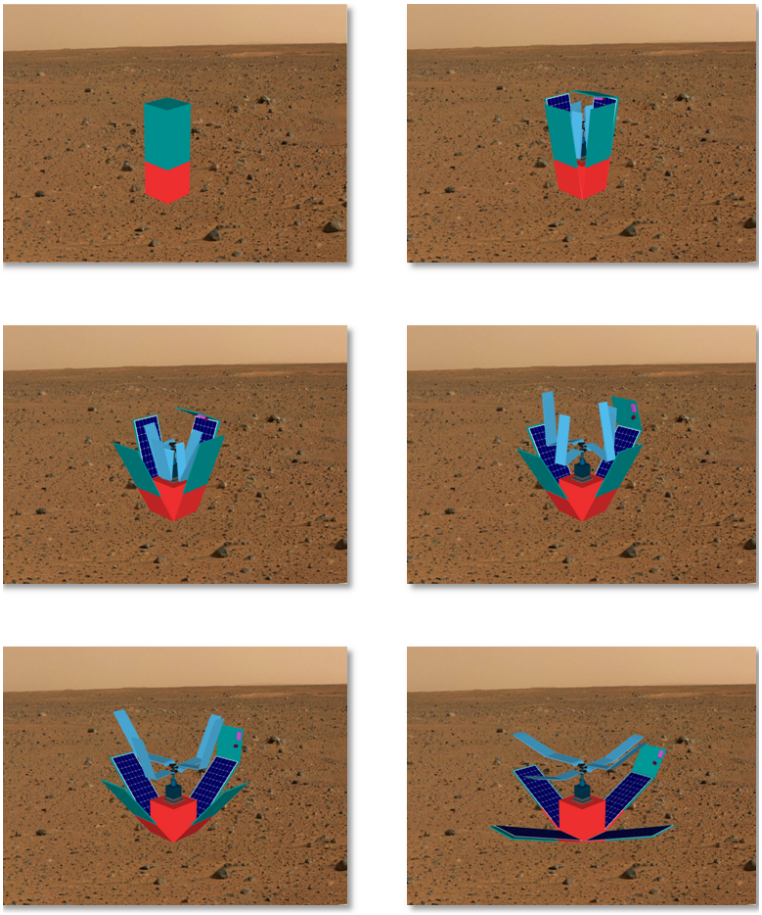

Figure 2: The sequence of unfolding operations of the Lander on the surface of Mars.

the selection of launch and arrival dates. Fig. 4 shows the daily average maximum and minimum atmospheric temperatures close to the ground as functions of time (represented by the solar longitude L_s from 0° to 360° over one Martian year) and geographical latitude (from the South pole at −90° to the North pole at +90°). The strong variations (absolute minimum temperatures are close to −130°C, whereas the maxima can reach 20°C) are closely associated to the relatively high eccentricity (0.0934) of the orbit of Mars, which causes an appreciable variability of the solar irradiation received by the planet. The figure

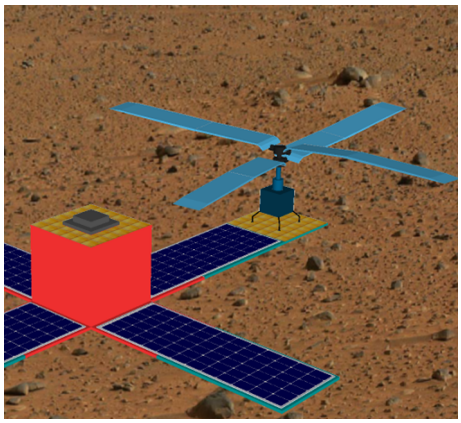

Figure 3: The deployed Lander with the two payloads at their respective positions at the beginning of surface operations: a simplified representation of the DPA on top of the avionic module in the center, and the AD on the recharging pad at one of the tips of the deployed structure.

shows that the most favorable thermal conditions occur in winter (solar longitude between 270° to 360°) in the southern hemisphere. However, the Martian meteorological conditions are severe at this epoch because the heat transport in the atmosphere causes strong air currents and winds which raise the dust from the ground causing devils and even planetary-scale storms. Therefore, landing close to the equator (the milder region on a yearly basis) at solar longitude earlier than 180° (beginning of autumn) is desirable. These considerations have been assumed in the form of requirements on the design of the trajectory and on the selection of launch and arrival dates (see Sect. 4). The exact location of the landing site has not been decided yet. It will be the object of further analysis and discussion at more advanced stages of the project.

3. The payloads

SMS exploits a modular architecture consisting of two main elements: the Lander, including the payload and avionic modules, and the DHS. The payload module hosts the AD in folded configuration, preserving its integrity during the

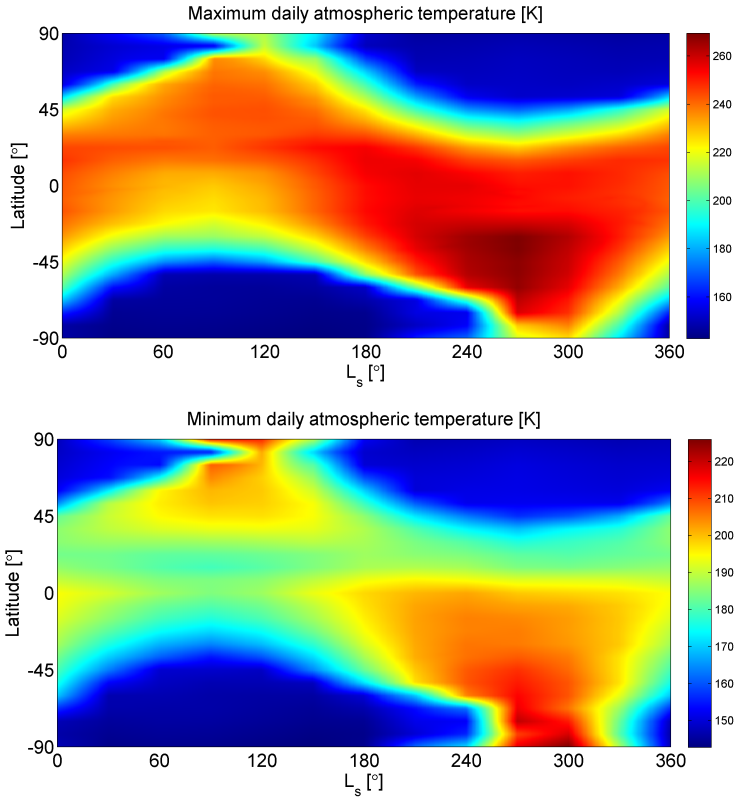

Figure 4: Daily average maximum (top) and minimum (bottom) Mars atmospheric temperatures close to the ground as functions of solar longitude L_s (over one Martian year starting at the Spring equinox, x-axis) and geographical latitude (from the South pole at $-90°$ to the North pole at $+90°$, y-axis).

transfer and allowing for its release after landing. The avionic module contains the DPA.

3.1. The aerial drone

Several studies in the open literature suggest that the next stages of Mars exploration will take advantage from the adoption of aerial drones [13, 14, 15, 16, 17, 18, 19, 20, 21, 22] since they can overcome some limitations inherent to rovers, such as the limited mobil-

Table 1: Mission requirements mapping on different aerial drone configurations.

Criterion	**Fixed-Wing Conventional Aircraft**	**Fixed-Wing VTOL Aircraft**	**Rotorcraft**
High-Resolution Imaging	Yes	Yes	Yes
Regional-Scale Survey	Yes	Yes	Limited
Controlled Flight	Yes	Yes	Yes
High-Volume Data Transmission	No	Yes	Yes
Multi-Mission Capability	No	Yes	Yes
Deployment Complexity	Higher	Higher	Lower

ity and the difficulty to explore rough terrains or canyons. Indeed, in an ideal scenario the exploration task should be distributed among drones and surface rovers. Drones provide higher flexibility, multi-mission and sample return capability by exploiting vertical takeoff and landing, and allow for local and/or regional-scale coverage and high-resolution imaging of Mars surface. Actually, low-altitude flight and multi-mission capability, as well as the use of swarms, would allow providing high-resolution imaging and wide area coverage at the same time. In this framework, the experiment designed for SMS aims at demonstrating the feasibility of releasing and flying an aerial drone on Mars, the capability of collecting high-resolution images of the surface using the Lander as the ground station for drone operation and recharging between flights, and performing multiple missions (i.e.,

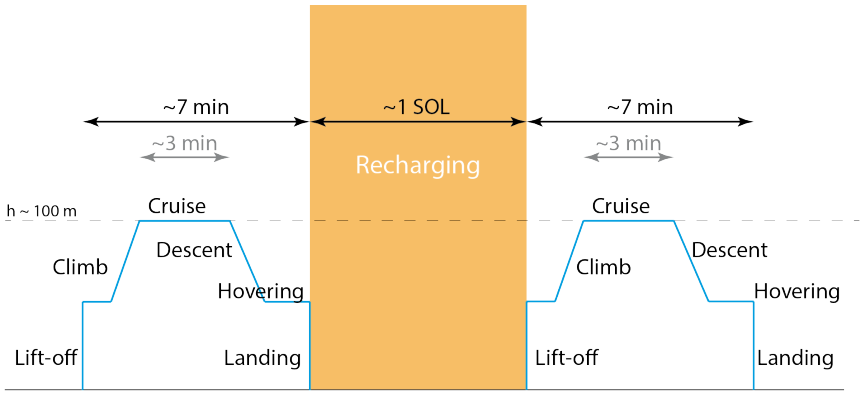

Figure 5: Preliminary mission profile of the AD showing two consecutive flights separated by a recharging interval of one Sol. Each flight consists in liftoff, climb, cruise, descent, hovering and landing.

multiple takeoffs and landings). After comparing different types of vehicles (see Table 1) on the basis of criteria such as high-resolution imaging capability, regional-scale survey performance, flight controllability, data volume transmission, multi-mission capability and deployment complexity, a rotorcraft configuration has been selected, since it satisfies the majority of the criteria at an acceptable level of technological complexity. However, it has to be noted that rotorcraft are slow in cruise and consume high power levels since the rotor must generate lift and forward thrust at the same time. Besides, rotorcraft offer a limited surface for installing solar cells for battery recharging. These problems can be overcome with a fixed-wing Vertical Takeoff and Landing (VTOL) configuration, which combines the vertical flight capability of a rotorcraft with the advantage of a fixed wing during cruise. However, VTOLs are more complex to deploy and heavier than an ordinary rotorcraft.

Designing of a rotorcraft for Mars is demanding due to the specific atmospheric and flight conditions, characterized by low Reynolds numbers and high

subsonic Mach numbers. In addition, although the surface gravity is only one third the gravity on Earth, the atmosphere is very thin (the density being about 1% of that on Earth at the surface). For these reasons, the sizing of the blades is a critical issue, which must comply with the packing requirements inside the payload module of SMS and with the need for sufficient volume, mass and power to complete its mission. Hence, the possibility of flying a drone on Mars also relies on the possibility of using lightweight materials (e.g., carbon fiber materials), high-specific energy power systems and miniature devices and components based on MEMS and CMOS technologies. All these issues have been considered in the selection process for the drone configuration and in the preliminary design. Specifically, if a coaxial configuration with counter-rotating blades is chosen, the rotor radius R is given by [23]

$$R = \frac{1}{\sqrt{n_{rot}}}\sqrt{\frac{W}{\pi DL}}. \tag{1}$$

Here DL is the rotor disk loading, W is the drone weight and n_{rot} is the number of rotors. With respect to conventional single-rotor and quadrotor architectures, the coaxial configuration offers mechanical and aerodynamic advantages, such as easier packing and deployment, smaller disk area, and no need for a torque balance device [23]. As for the propulsion, an electrical engine seems the best choice, since it can be recharged using solar cells. Of course, without a fixed wing, the surface available for photovoltaic cells is very limited, thus secondary batteries must be used to sustain the electrical engine during flight. The batteries can be recharged using the solar arrays of the Lander or using the solar cells installed on the blades. In the preliminary design, it has been assumed that battery recharging is carried out at the Lander, the options of the solar cells on the blades being left for future studies. The drone design has been tailored to the preliminary mission profile outlined in Fig. 5, whereas the physical and performance parameters are summarized in Tables 2 and 3. The total mass of the AD is of 7 kg, whereas the size of the main body is 0.20 m $\times$ 0.15 m $\times$ 0.15 m. The electric power is provided by four LiPo battery modules which can be recharged in about one Sol, **thanks to a recharging pad [24], integrated**

Table 2: Sizing and performance parameters of the AD.

Parameter	**Value**	**Units**
Design density	0.0167	kg/m^3
Mars viscosity on the ground	$1.289 \cdot 10^5$	kg/ms
Mars speed of sound	230	m/s
Number of rotors	2	-
Rotor radius	1.25	m
Cruise altitude	100	m
Forward speed	11.5	m/s
Single disk loading	1.3	kg/m^2
Tip Reynolds number	57500	-
Blade solidity	0.1585	-
Flight time	7	min
Mach number at blade tip	0.64	-
Total power consumption	410	W
Total energy consumption	60	Wh

Table 3: Mass budget of the AD. **TMS stands for Thermal Management System.**

Subsystem	**Mass (kg)**
Fuselage & landing gear	1.2
Drive & hub	1.0
Power supply	0.5
Blades	2.5
Avionics, Payload & TMS	1.8

into the lander lateral surface, on which the drone has to land (Fig. 3). Each flight lasts seven minutes distributed among liftoff, climb, cruise, descent, hovering and landing. In the cruise phase, which lasts three minutes, the drone flies in a single circular path with a radius of about 320 m at an altitude of

100 m around the location of the Lander. The forward speed is of 11 m/s and the ground range reaches a value of 2 km approximately. This flight profile has been selected to preserve line-of-sight contact with the Lander, that acts as a ground station. The AD hosts a payload, i.e., an imaging camera (CAM), with the twofold function of taking high-resolution (i.e., cm-level) pictures of the surface and as aiding sensor for autonomous navigation, providing optical flow (OF). The images are transmitted to the Lander and then to Earth. The selection of the camera has been conducted through trade-offs among requirements, image resolution, weight and size. The candidate is a COTS, low-weight (400 g), low-power-consumption (4.5 W) camera produced by Point Grey [25]. **A precise navigation system is required to make the AD land correctly and autonomously on the charging pad. To this aim, technical solutions already exploited for terrestrial drone flying in GPS-denied environment have been considered for Mars drones [26, 27]. These solutions rely on vision-aided inertial navigation (i.e., the fusion of inertial and optical flow measurements within an Extended Kalman Filter, EKF), which is augmented by sun line measurements provided by onboard sun sensors (SS), altitude measurements provided by a barometric sensor (BARO) and ranging measurements provided by the radio-link channel between the AD and the Lander, which serves as ground control station. The proposed autonomous navigation concept is illustrated in the block-diagram of Fig. 6. According to the mission profile of Fig. 5, the AD is assumed to fly a circular path around the Lander location, thus providing line of sight and direct link with the lander.**

3.2. The dust particle analyser

The monitoring of airborne dust is very important in Martian climatology. The dust absorbs and scatters solar and thermal radiation, and this in turn affects the atmospheric thermal structure, balance and dynamics (in terms of circulation). Even in moderately dusty situations, the influence of dust on

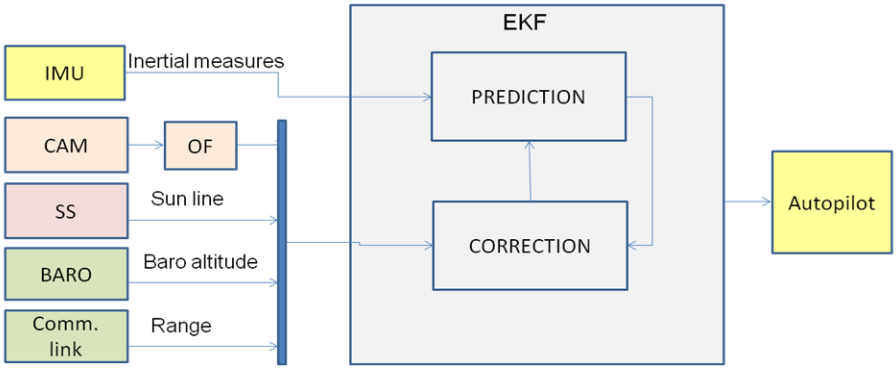

Figure 6: **Autonomous navigation scheme (concept).**

the Martian thermal structure is critical. During regional or global dust storms, more than 80% of the incoming sunlight is absorbed by the dust, causing intense atmospheric heating. Airborne dust is therefore a crucial climate component on Mars, with influences on the atmospheric circulation at all scales. The main dust parameters affecting the atmospheric heating are the size distribution and abundance. Moreover, wind and windblown dust represent nowadays the most active processes with long-term effects on the Martian geology and on the morphological evolution. Aeolian erosion, dust redistribution on the surface and weathering are mechanisms that couple the surface and atmospheric evolution and are driven by the wind intensity and the grain properties. In this context, it is clear that the knowledge of the atmospheric dust properties and the mechanisms of dust settling and raising into the atmosphere are important to the understanding of the Martian climate and surface evolution.

The size distribution is generally measured indirectly through remote sensing data. However, these measurements are related to the entire atmospheric column and give poor information on the atmospheric layer close to the surface, where dust is lifted. The DPA will be able to perform for the first time measurements of dust concentration directly on the Martian soil. The DPA envisaged as scientific payload for SMS can be classified as an optical particle

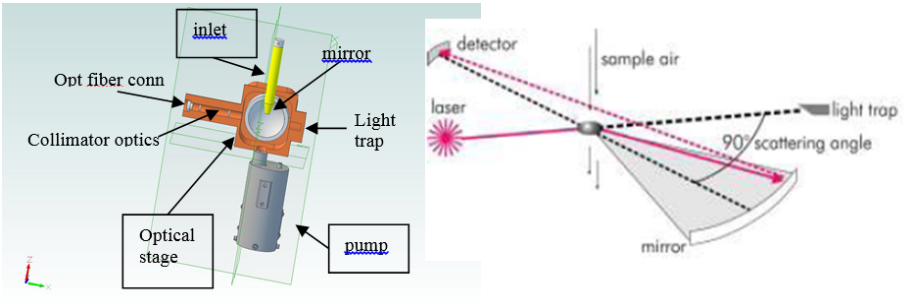

Figure 7: DPA's working principle.

counter: it processes the light scattered from the single dust particle to measure its size and estimate the abundance of each species. A proper fluid-dynamic system, implemented in the instrument and including a pump and a sampling head, allows the sampling of the Martian atmosphere with the embedded dust.

The DPA's working principle is reported in Fig. 7. The pump samples the Martian atmosphere, generating a flux of gas and dust across the instrument through the inlet. When the dust grains reach the optical sensor, they cross a collimated laser beam emitted by a laser diode. The light scattered by the grains is collected by a mirror and sent to a photodiode, whose output signal is amplified and processed by the electronics of the instrument. Eventually, the flow of air and dust is ejected back into the atmosphere.

The instrument measures the size of atmospheric dust in the range from 0.2 to 10 μm radius, with a factor of coincidence lower than 4%. Once the particle counts and size measurements have been performed, the dust number density can be derived, since the volume sampled by the instrument is known. The system has been designed in order to work with particle concentrations up to several hundreds per cm^3 before coincidence effects become significant. The estimated fraction of coincidences ranges from 0.01% (in the presence of haze) to less than 4% (in the case of a dust devil).

The current design of the DPA is derived from the MEDUSA instrument, selected for the ExoMars Humboldt payload [11] (which reached a TRL of 5.2).

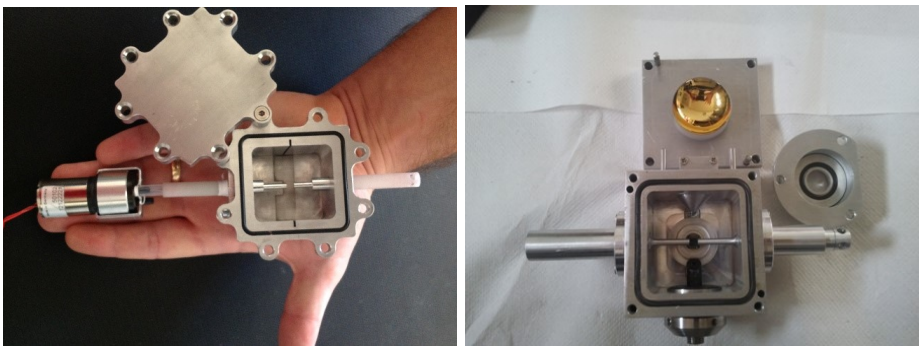

Figure 8: Left: breadboard for the fluid-dynamic test; Right: functional breadboard.

The current new design is strongly optimized and requires much less mass and fewer power resources. A laboratory breadboard (Fig. 8) of the instrument was developed with Italian Space Agency's (ASI) funds in 2011 and, later, by exploiting INAF resources. The breadboard was successfully tested, demonstrating the expected performances and reaching *de facto* a TRL between 4 and 5. All the components of the breadboard are COTS that can be space qualified. Else, equivalent space-qualified elements can be found on the market. Only the pump used in the breadboard is a commercial pump that has no space-qualified version. For this reason, it will be completely redesigned to fulfill the requirements imposed by the space environment. Tests for the verification of fluid-dynamic aspects, together with performance tests on the integrated instrument were performed in a Martian simulation chamber at the INAF-OAC premises (Fig. 9). The tests were executed at a pressure equivalent to that of the Martian atmosphere close to the surface (6-8 mbar) and at ambient temperature. Dust particles were injected by means of a particle dispenser system, designed and implemented by INAF-OAC. Eight sets of mono-disperse latex particles with calibrated size were injected in the Martian simulation chamber. For each set, the output signal (i.e., the photodiode current) generated by more than 100 sampled grains was acquired and averaged. Eventually, the agreement of the acquired values with Mie's theory was verified.

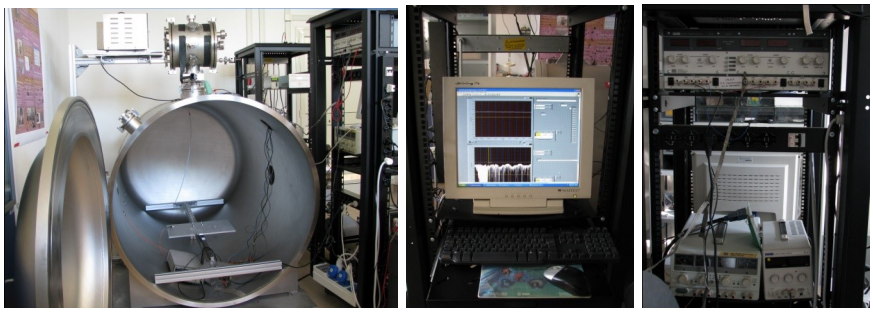

Figure 9: The Martian Simulation Chamber equipped with the Particle Injection System and the Power and Control Systems.

The DPA will be accommodated in a fixed position on the Lander (see Fig. 3). The possibility of embarking the DPA on the drone was analysed, but discarded, because this solution is more complex and does not ensure a significant increase of the scientific return. According to the current baseline design, the DPA will be activated after landing with at least four runs per Sol (one in the morning, two at midday, one in the evening - one run during the night is also desirable). The lifetime of the DPA will depend on the available resources of energy and data link. Longer and continuous acquisitions from the DPA can allow the detection of macroscopic phenomena of dust lifting, such as the dust devils. The possibility to trigger the DPA acquisition by means of other sensors, such as pressure sensors, can highlight this kind of phenomena as well. The possibility to perform measurements with the DPA during the descent phase of SMS will also be considered and will be object of study in the next stages of the project. The DPA has a total mass of 600 g (20% of margins included) and requires about 3 W of power. It interfaces digitally with the On-Board Data Handling (OBDH) system of SMS through a serial interface, and is controlled as a slave unit by the commands of the OBDH. The OBDH downloads the acquired data through an appropriate protocol. Scientific data can be either in the form of raw data, i.e., the complete waveform corresponding to the single event (dust grain), or transmitted in the form of histograms, an option which

is very useful to limit the data volume in case of narrow communications band.

4. Launch and interplanetary trajectory

Following an analysis of the time required for the development of the project, the interval 2020-2024 have been selected for the search of the launch date. The launch opportunities have been computed in a two-body Sun-spacecraft gravitational model, in which the planets are massless bodies revolving on secularly precessing Keplerian ellipses, as in the model by [28]. This approximation is suitable for preliminary analyses. The solution of Lambert's problem for the given range of dates and with a time resolution of one day has allowed to identify the opportunities for the Earth-to-Mars transfer. These opportunities form windows (the Porkchop plots, PCPs) which exhibit a periodicity of two years approximately, in agreement with the synodical period (2.14 years) of the two planets. Hence, three PCPs are available for the 2020-2024 interval, centered respectively in 2020, 2022 and 2024. The opportunities with the minimum cost at departure are those associated to the 2024 window, in particular those corresponding to type II trajectories (i.e., trajectories with transfer angles larger than 180°) (see Fig. 10). **The 334-days trajectory which leaves the Earth on 2 October 2024 (JD 2460585.5) and arrives at Mars on 1 September 2025 (JD 2460919.5) has a departure cost very close to the absolute minimum and a low arrival hyperbolic excess speed**. This solution is shown in Fig. 11. It has an Earth C_3 of 11.316 $\mathrm{km}^2/\mathrm{s}^2$ and a Mars v_∞ of 2.455 km/s. The arrival date (corresponding to $L_s = 135°$) satisfies the requirement of landing before the local Fall equinox.

C_3 sets the requirements on the wet mass of the spacecraft on the basis of the performance of the launcher. Following ESA's recommendations, the launcher has to be one of the three European vehicles, i.e., Ariane 5, Soyuz or Vega. Vega [29] is the cheapest and the smallest, in other words the most suitable for a small-class mission. Unfortunately, Vega launches to geocentric orbit ($C_3 < 0$) and does not achieve Earth escape [29]. A recent study [30]

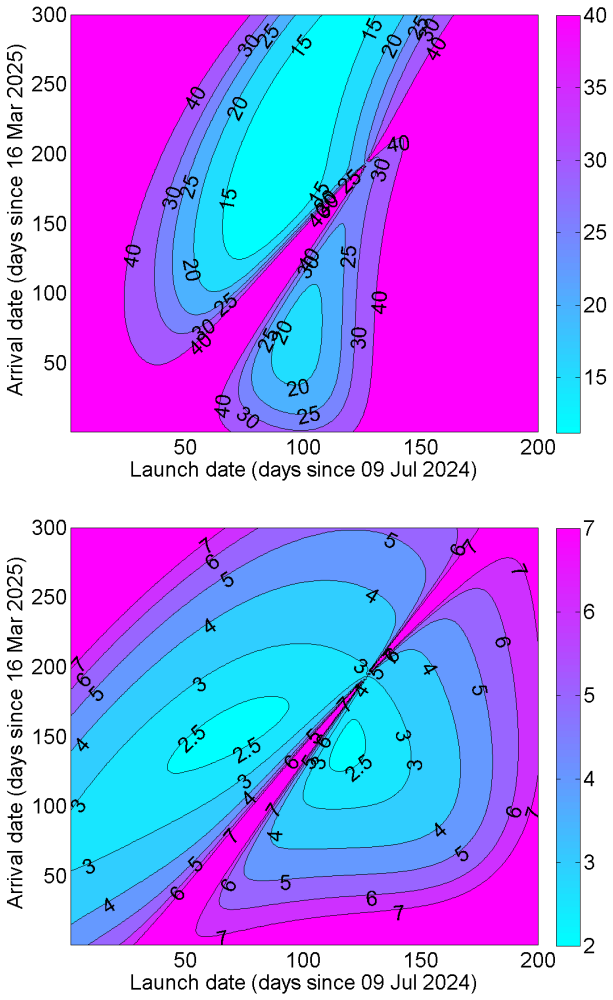

Figure 10: Porkchop plots describing the Earth-to-Mars direct transfer opportunities for the year 2024: contour lines of equal departure C_3 in $\mathrm{km}^2/\mathrm{s}^2$ (top) and arrival hyperbolic excess speed v_∞ in km/s (bottom). Each plot exhibits two minima, respectively, in the upper (long journeys) and in the lower (short journeys) half of the map.

illustrates the capability of Vega to launch interplanetary spacecraft thanks to an additional *ad hoc* bi-propellant fifth stage (i.e., the PM) with the escape performance shown in Fig. 12: injection into a 300-km LEO low-inclination orbit is assumed, and two options for the size of the fifth stage propellant tank

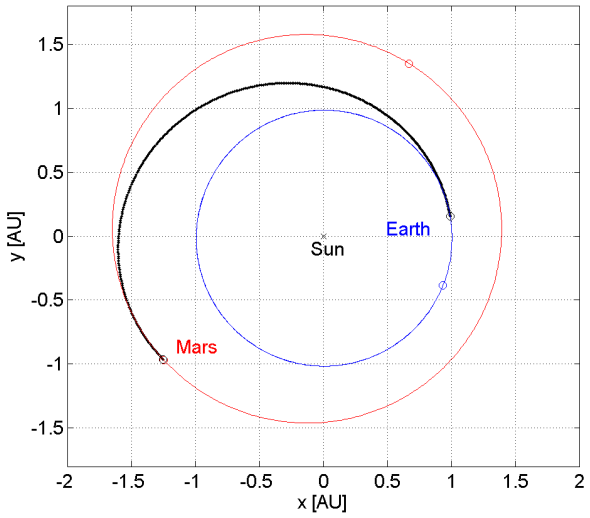

Figure 11: Baseline solution for the direct trajectory that shall take SMS to Mars. The left plot also shows the positions of the two planets at departure and at arrival.

are considered, i.e., short (yellow line) and long (red line). The Lisa Pathfinder mission [31] took advantage of this design, and successfully launched to the L_1 point of the Sun-Earth system: the PM was integrated with the spacecraft inside Vega's payload fairing and, upon separation from the fourth stage of the rocket, it executed a series of apogee raising maneuvers until escape was achieved. The baseline launch profile of SMS is very similar to this. Adoption of the long propellant tank allows to launch 320 kg of wet mass, margins included (see Fig. 12). The apogee raising sequence shown in Fig. 13 is just a simple exercise based on the example of Lisa Pathfinder. It shows that SMS can be injected into the right hyperbolic trajectory by means of six successive perigee burns of 0.4249 km/s, followed by a final burn of 0.8297 km/s of 22 minutes duration.

The interplanetary trajectory of Fig. 11 targets the center of Mars in a two-body Sun-spacecraft model. The gravitational influence of the planet gradually takes over as SMS approaches its destination. According to the patched conics model, the trajectory is determined solely by the planet's gravity once an ideal border, i.e., the surface of the sphere of influence (SOI, 580 000 km radius), is

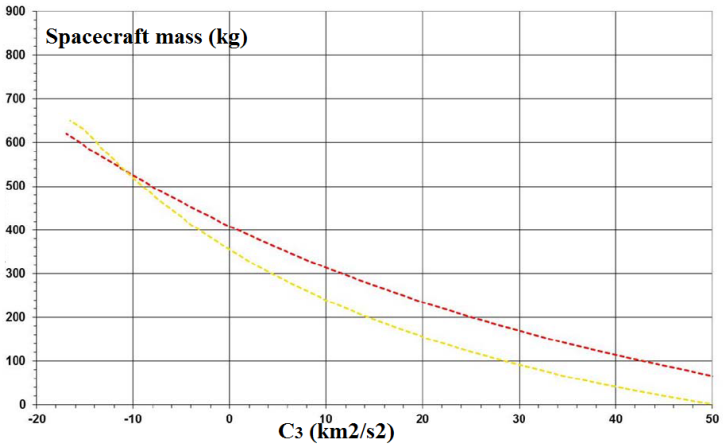

Figure 12: Approximate escape performance for a Vega launch with the PM, assuming insertion in a 300 km low-inclination LEO orbit [30].

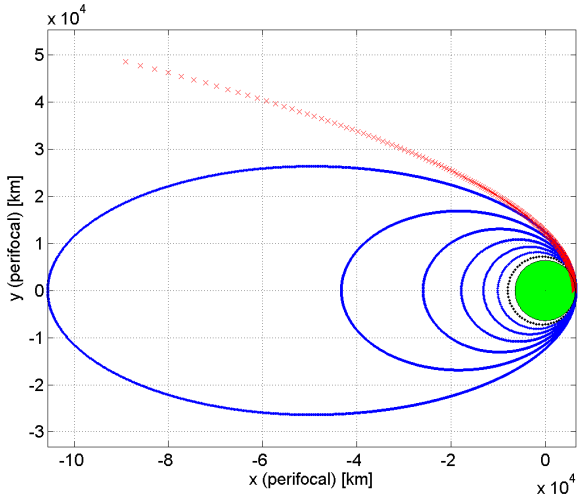

Figure 13: Example of a possible apogee raising sequence to be executed by the PM: six intermediate elliptical orbits with increasing semimajor axis and apogee radius (thick curves) until escape on a hyperbolic trajectory is achieved (crosses).

crossed. The resulting Mars-centered hyperbola must be appropriately corrected in order to satisfy the aerodynamic requirement that the flight path angle be

in the range $[-14°, -12°]$ at an altitude of 125 km over the surface, assumed to be the upper limit of the Martian atmosphere. The correction maneuver is modelled as an impulse applied at SOI crossing by the on-board propulsion system (see Sect. 7.4). With a magnitude of 33 m/s, this impulse makes SMS enter the atmosphere at a speed of 5.5 km/s and land close to the equator, as desired.

5. Entry, descent and landing

The feasibility study of SMS includes the definition of the atmospheric entry trajectory, a preliminary assessment of the flight characteristics and the trajectory evaluation until landing. Velocity, Mach number and pressure profiles have been computed over the entry trajectory using 3-DoF models and the Newtonian theory for hypersonic flow. Heat fluxes have been estimated along the trajectory using engineering formulations [32]. Given the extremely low density of the Martian atmosphere, entry vehicles need a low ballistic coefficient to decelerate and obtain a safe landing speed. All past Mars landers have employed similar EDL methods to safely touch down [33]: the entry capsule has a fore body-fixed heat shield to protect the lander in the high-aerodynamic-heating portion of the flight; then, when the capsule reaches supersonic speeds, a parachute system is deployed to slow down; once at subsonic speed, the heat shield is jettisoned and a second, subsonic parachute is deployed; eventually, either an active (thrusters) or a passive (airbags) touch down technology is employed to achieve soft contact. The case of SMS presents an important difference: the umbrella-like deployment system for the heat shield allows to decrease the ballistic coefficient to less than 20 kg/m^2, i.e., less than one third the value of all previous landers [34]. This fact brings several advantages over those missions:

- a reduction of the aerodynamic and aerothermodynamic loads along the hypersonic entry flight path;
- a single subsonic parachute may be sufficient since the capsule reaches subsonic speeds at higher altitudes;

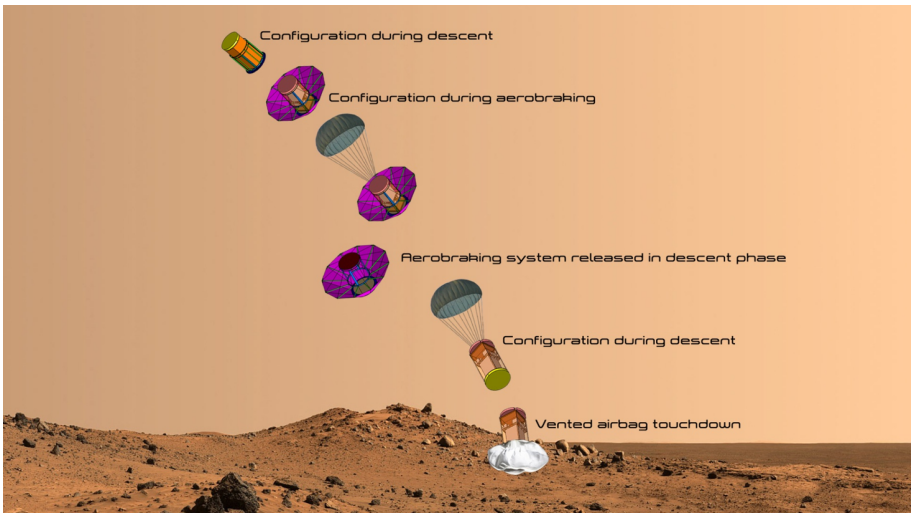

Figure 14: **Artistic representation (not to scale) of the main events along the EDL of SMS.**

- thanks to the lower speed obtained close to the ground, the energy of the impact can be absorbed by some passive system (e.g., an airbag or a crushing system) only.

Combining two innovative EDL systems, i.e., the DHS and a passive energy absorber, may seem rather risky. However, the former technology is going to be flight tested in 2018 by Earth re-entry after ascent on board a suborbital sounding rocket [9, 35]. The flight shall verify the deployment mechanism, the telescopic spreaders and the jettisoning system. Several laboratory experiments have been conducted on the materials and a qualification plan of the system is under execution. These activities should mitigate the technological risk associated to the heat shield.

Figure 14 outlines the main events of the EDL. It is worth noting that the deployment of the shield allows to decelerate to subsonic speeds at high altitude so that a subsonic parachute can be exploited to further reduce the descent speed to values compatible with a passive soft landing system.

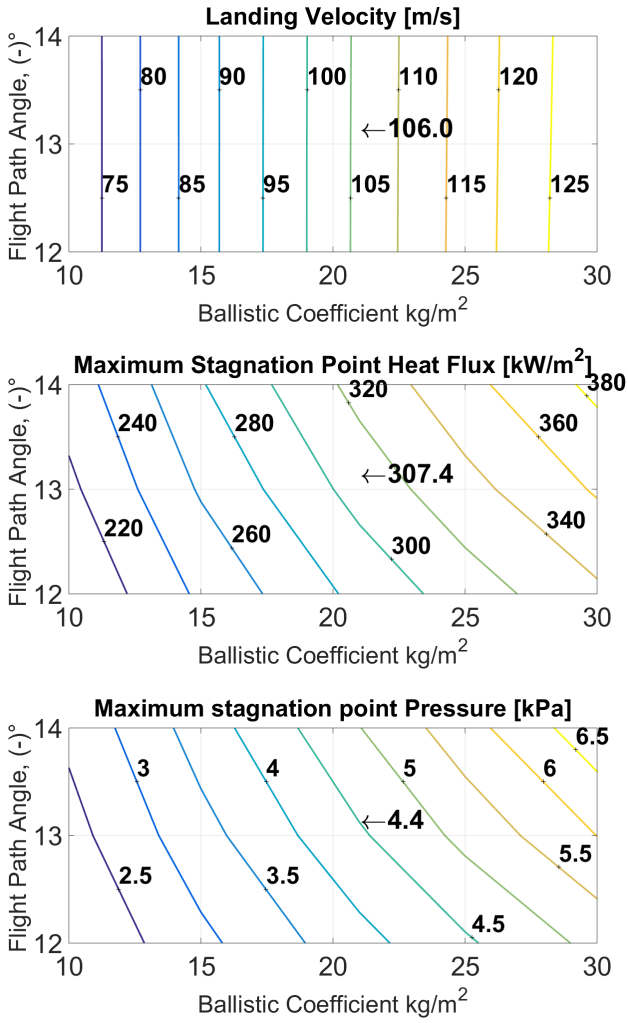

Figure 15: Landing speed (top), stagnation point heat flux (middle) and stagnation point pressure (bottom) as functions of ballistic coefficient (x-axis) and entry flight path angle (y-axis).

400 The evaluation of the aerodynamic design parameters has been carried out through a parametric analysis based on varying the ballistic coefficient and the flight path angle (Fig. 15). The initial entry speed (as obtained from the approach trajectory design, Sect. 4) is of 5.5 km/s and the entry altitude is of 125 km (this value is generally accepted as the height of the upper limit of the

Martian atmosphere). The entry mass is of 150 kg and the diameter of the deployed DHS is of 3 m, whereas for the drag coefficient a value of 1 is assumed. The case of ballistic coefficient equal to 21 kg/m^2 and entry flight path angle of $-13°$ is particularly interesting for the case of SMS and is highlighted in the figure.

A comparison with the parameters of the entry trajectories of previous Mars landers [34] has been conducted. As a whole, Figure 16 shows that the lower ballistic coefficient achieved by SMS yields a lower stress in terms of aerodynamic and aerothermodynamic loads. Furthermore, one of the most important results achieved using the umbrella-like deployable system is the possibility of reaching the subsonic regime at altitudes close to 15 km without the need for complex deceleration technologies (such as supersonic parachutes, thrusters or ballutes). This feature provides flexibility, and the unique possibility to land at higher altitudes (i.e., higher than MOLA 0 level) with a low-cost system.

In order to assess the landing performance with a single parachute in subsonic regime, a parachute analysis has been carried out. The analysis is based on 3-DoF models and varies the exposed surface according to several parachute diameters. Due to the lack of knowledge about the behavior of subsonic ringsail parachutes in the atmosphere of Mars, a preliminary analysis has been executed using the diameters of Disk-Gap-Band parachutes tested on previous Mars landers [33]. The deployment of the parachute in subsonic regime is simulated by introducing the parachute at an altitude of 10 km, where the Mach number has an expected value of 0.75. The drag coefficient has been set at 1 [36]. After parachute deployment, the DHS is jettisoned causing a mass reduction. This fact has been taken into account by evaluating the variation of the landing speed as a function of mass, for the four values of the diameter of the parachutes used in the previous Mars missions [33] (Fig. 17). A detailed sequence of parachute deployment and DHS separation will be defined in a subsequent phase of the study.

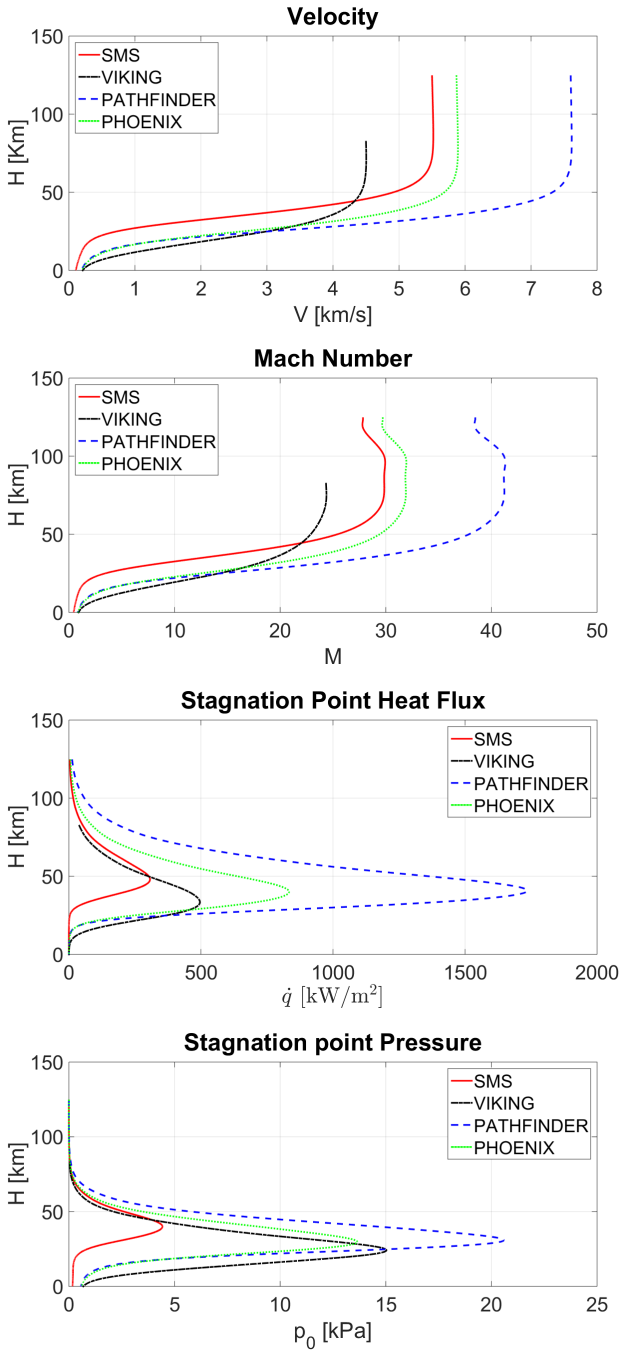

Figure 16: Speed, Mach number, stagnation point heat flux and stagnation point pressure for the case of SMS and of three previous Mars landers (Mars Viking, Mars Pathfinder, Phoenix).

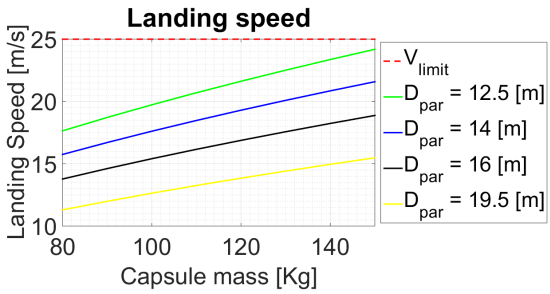

Figure 17: Landing speed as a function of capsule mass and parachute diameter (D_{par}).

Finally, an aerothermodynamic analysis on the selected configuration allows to estimate the aerodynamic and thermal field around the entry capsule and, in particular, on the flexible (deployable) and rigid elements of the surface of the thermal protection system. Depending on the flow regime, different numerical state-of-the-art codes have been employed. In a continuous regime, the classical Navier-Stokes and energy equations have been solved using the commercial code STAR-CCM+ [37]. The flow field around the capsule is assumed laminar. Due to its chemical composition (95% carbon dioxide), the atmosphere has been treated as a single-component ideal gas. The numerical simulations have been performed with a density-based, time-implicit numerical solution scheme through a control-volume-based technique. The AUSM (Advanced Upstream Splitting Method) scheme for convective numerical fluxes has been employed. This procedure has been successfully applied to similar problems by [38, 39]. In a rarefied regime, the study of the aerodynamic characteristics requires Direct Simulation Monte Carlo (DSMC) [40, 41]. A two-dimensional axisymmetric analysis has yielded the distribution of the thermal and mechanical loads on the surface of the lander, thus allowing a comparison with the results of the EDL assessment. Three-dimensional examinations have provided the temperature and pressure distributions on the three-dimensional geometry under the most severe conditions along the entry trajectory. Figure 18 shows good agreement in terms of stagnation point pressure prediction. This means that Newtonian theory is

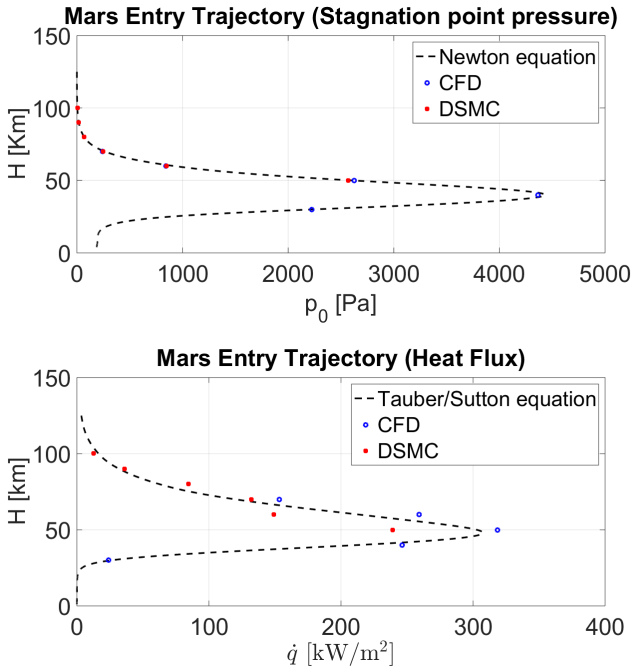

Figure 18: CFD, DSMC and hypersonic Newtonian theory (top) and Tauber/Sutton theory (bottom).

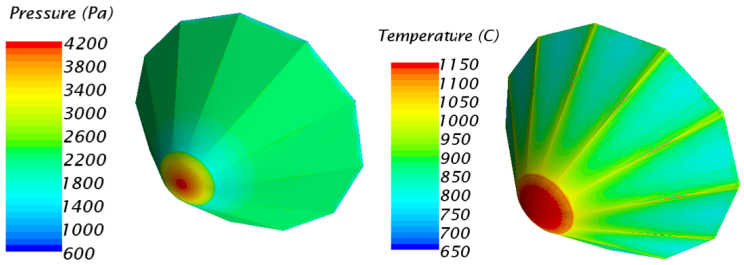

Figure 19: Left: pressure distribution at maximum stagnation point pressure at 40 km altitude; Right: temperature distribution at maximum stagnation point heat flux condition at 50 km altitude.

a valuable tool to predict the stagnation point pressure for a blunt body in a hypersonic flow field. As for the stagnation point heat flux, it is a known fact that the precise evaluation of this parameter over the planetary entry trajec-

tory is a very hard task. As shown in Figure 18, the more rarefied the flow regime the closer the DSMC results are to the curve predicted by the theory, whereas the lower the altitude (towards the continuum flow regime) the closer the CFD code results are to the prediction of the Tauber/Sutton equation. Finally, Figure 19 shows the pressure and temperature distributions, respectively at maximum stagnation point condition and at maximum stagnation point heat flux condition along the entry trajectory.

6. The deployable heat shield

The main component of the DHS is a flexible shield (FS), whose deployment mechanism is essentially made up of a sliding structure, tensioning poles and threads. Figure 20 shows the shield in retracted (top) and deployed (bottom) configuration, the Lander being the parallelepiped body in the center. A rigid nose cone and the associated support structure are also part of the DHS.

The FS is made of woven ceramic fabrics. Specifically, NextelTM Aerospace Fabrics 312 are woven from strong, continuous alumina-borica-silica fibers, and are designed to pass the FAA 2000°F 15-minute flame penetration test. They retain strength and flexibility, with little shrinkage at temperatures lower than 1100°C. The shield consists of two 0.38-mm layers, each composed by twelve trapezoidal patches reinforced at the edges (see Fig. 21). When deployed, the shield approximates a 45° conic surface, with a maximum diameter of 3.11 m and a maximum working temperature of 1300°C. The fabric layers are put in tension by twelve poles and are clamped at the nose cone support structure.

To reduce the overall system mass, a hollow configuration has been used for the nose cone, which offers also the possibility of accommodating the airbag (or part of it). To increase the nose cone strength, a double-layer solution has been adopted in which the external layer is made of RESCOR 310M (a silica foam) with a thickness of 4 mm and a maximum working temperature of 1650°C, and the inner layer is made of a FW12 Oxide/Oxide ceramic matrix composite with a thickness of 2 mm and a maximum working temperature of

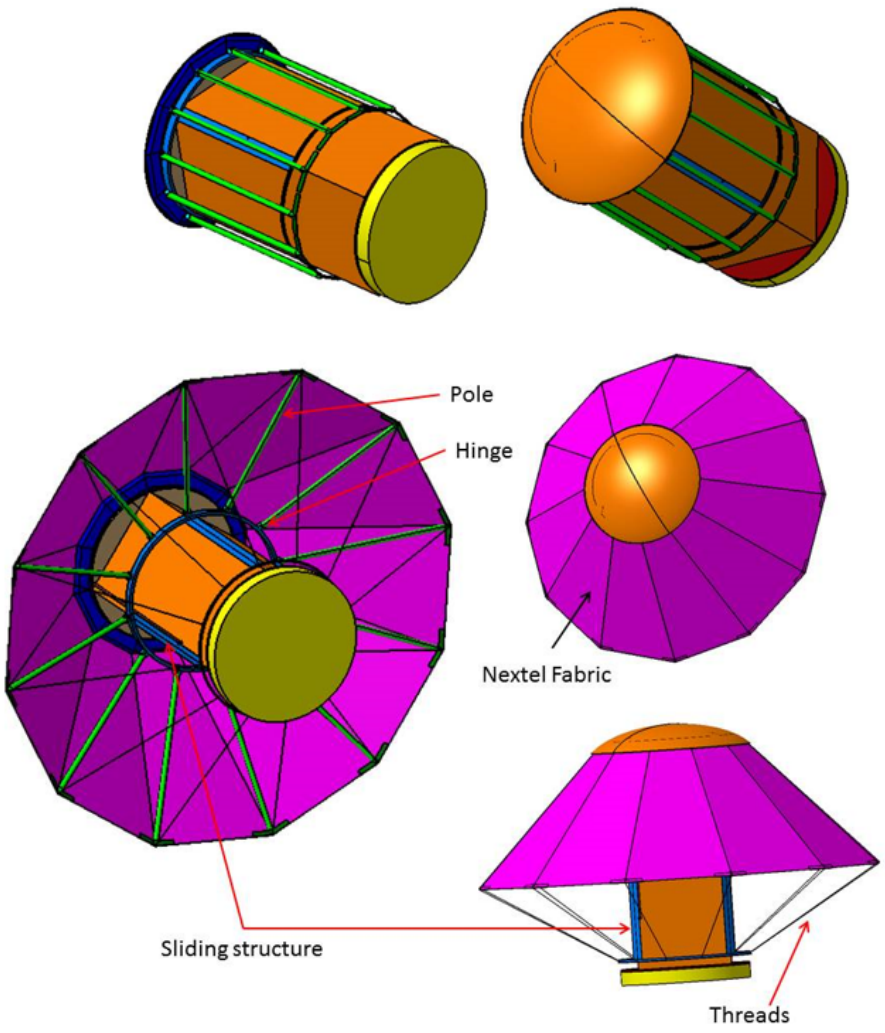

Figure 20: DHS layout in retracted (top) and deployed (bottom) phase.

1300°C. Actually, the temperature reached at the nose during entry is equal to the maximum working temperature of FW12, but the temperature at the inner layer is lower due to the 4-mm RESCOR layer. The deployment mechanism, made of titanium alloy Ti6Al-4V, is composed by a sliding structure consisting of two rings, connected by four rods, sliding along the Lander. The twelve

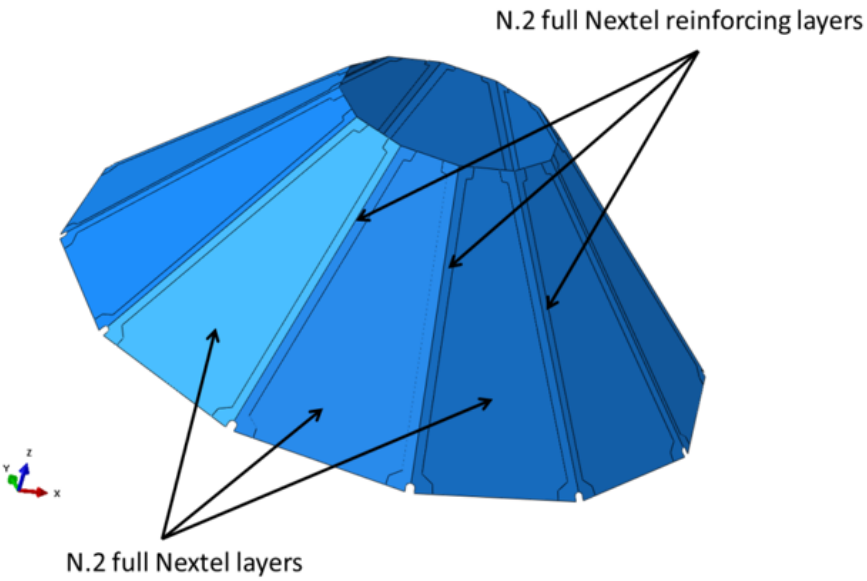

Figure 21: Layout of the flexible shield.

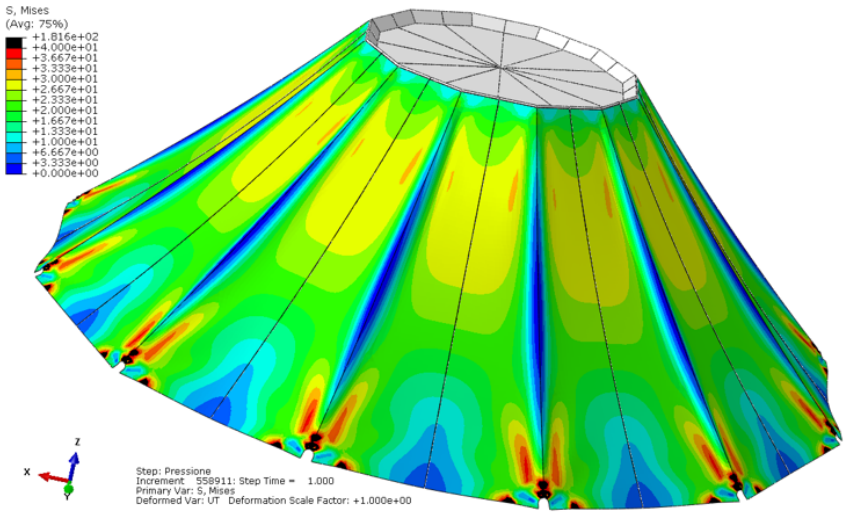

Figure 22: Stress map on the Nextel Fabric during entry.

tensioning poles (50 mm diameter, 1 mm thickness) are connected to the upper ring by means of cylindrical hinges, while the lower ring supports one end of the twelve lower threads (1.5 mm diameter). The lower and upper threads (4 mm diameter) ensure fabric stabilization in the tensioning phase before the entry. Indeed, under pressure loads the lower threads lose tension, while the upper threads support the fabric in sustaining the loads. The deployment system is completed by two electric actuators, which allow the displacement of the sliding structure during the opening phase. The shield design has been verified by using a nonlinear finite-elements simulation model of the flexible shield and of the main structural parts of the deployment mechanism, considering load conditions deriving from the tensioning phase and entry (pressure loads). Specifically, the main load acting on the nose cone is the pressure during the entry phase. Values of 4.4 kPa and 3.2 kPa have bee used for the pressure, respectively on the nose and on the fabric, as predicted by the aerothermodynamic analysis. Also the tensioning load has been simulated. The deployment mechanism has been verified under the loads deriving from the deployment of the flexible shield and the entry pressure loads. Figure 22 shows the stress distribution of the Nextel fabric during entry: the stress level is lower than the allowable limit (40 MPa) except in very small areas (i.e., the small black areas in the figure). These areas can be reinforced with a slight modification of the fabric design. The maximum deformation experienced by the fabric is of 42 mm, a value much smaller than the shield diameter.

7. Subsystems design

This section provides a short description of the main accomplishments related to the system's budgets and subsystems design. It is worth outlining that, as common in the early stage of a project, for some subsystems (e.g., the thermal control subsystem) solutions and parameter values have been taken from the relevant literature.

7.1. Mass budget

To reduce costs and risks, the overall system design exploits the heritage of past and currently planned Mars missions, as well as COTS components and units. Table 4 reports the dry mass breakdown for the three main components of the system, i.e., the CS, the Lander and the DHS (see Fig. 1 left). Following ESA's margin philosophy, a 20% margin has been added to the total dry mass of 241.3 kg, yielding a value of 289.6 kg. A value of 14.8 kg for the propellant mass is required for maneuvering during the cruise and up to Mars entry point. This yields a system wet mass of 304 kg, leaving a margin of about 5% with respect to the capabilities of Vega endowed with the PM for a C_3 of 11.3 km^2/s^2.

Table 4: System's mass breakdown. The meaning of the abbreviations is as follows: S&M = Structure & Mechanisms; OBDH = On Board Data Handling; GNC = Guidance, Navigation & Control; TPS = Thermal Protection System.

Cruise stage	Mass (kg)	**Lander**	Mass (kg)
Propulsion	7.8	X-band Telecomms	9.7
Attitude Determination	0.6	UHF Telecomms	3.0
Telecomms	1.1	Thermal Control	8.0
Thermal Control	10.8	Electrical Power Subs.	16.8
Electrical Power Subs.	7.2	OBDH	3.1
S&M	43.2	S&M	22.8
Harness	3.5	GNC	3.3
Total dry mass	**74.2**	Payloads	7.9
Deployable heat shield		Parachute System	10.4
Structure	36.7	Soft Landing System	19.8
Nose cone	10.2	Harness	5.2
TPS	10.2	Total dry mass	**110.0**
Total dry mass	**57.1**		

7.2. Electrical power subsystem

The electrical power budget has been developed considering the following main phases: launch, apogee raising, interplanetary cruise, EDL and surface operations. Surface operations include the flights and the recharging of the AD and the activities of the DPA. Table 5 summarizes the energy requirements in the several phases. It is worth outlining that the apogee raising operations consist of six intermediate elliptical orbits, the lowest of which suffers the longest eclipses (32 minutes duration).

Table 5: The electrical energy (Wh) to be provided, respectively, by the CS and by the Lander in the several phases of the mission.

	Launch	**Raising (sun)**	**Raising (eclipse)**	**Cruise**	**EDL**	**Surface (day)**	**Surface (night)**
CS	2	718	164	476721	-	-	-
Lander	128	27863	239	907608	53	1304	668

The electrical power subsystem is a photovoltaic system. Solar energy is available during apogee raising, interplanetary cruise and day-time surface operations on Mars, whereas during the eclipses of the apogee raising maneuver (Fig. 13), during EDL and in the Martian nights the power is provided by a Li-Ion battery. The sizing of the system has been made according to the worst-case power requirements of the several phases (which vary between 70 W for Martian night survival and 230 W for full daytime operations) and taking into account the several configurations that the spacecraft takes over the mission. For this reason, solar cells are present both in the CS and in the Lander: in particular, during apogee raising and interplanetary cruise, only the CS solar array can work and the Lander solar array stays folded, whereas once on the surface of Mars, only the latter is available because the CS is released prior to atmospheric entry. The CS solar array occupies the bottom surface and part of the lateral surface of the stage (see Fig. 23). The Lander solar array covers the inner side of the lateral surfaces (rectangles) of the structure (see Fig. 3). The battery is hosted by the avionic module of the Lander.

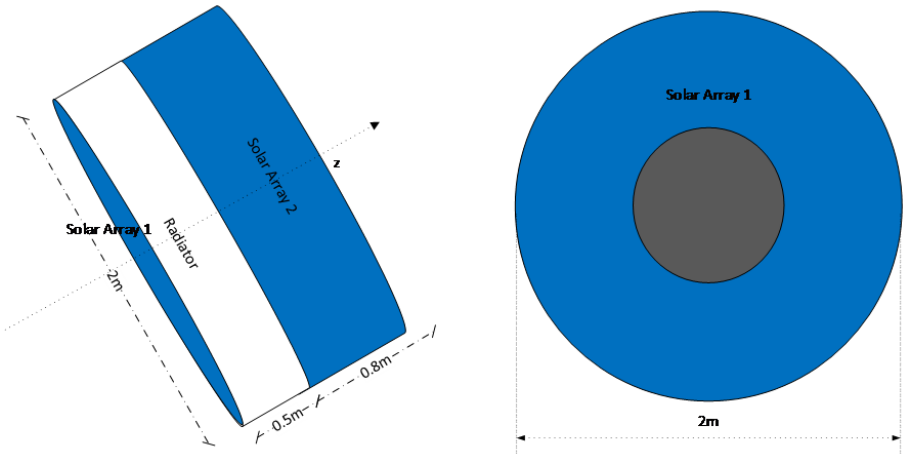

Figure 23: Solar cells on the external surface of the CS: side (left) and bottom (right).

7.3. Communications

During cruise, communications are guaranteed via either the low-gain antenna (CLGA) or the medium-gain antenna (MGA) of the CS. The CLGA is useful in the first few weeks after launch (due to the large Sun-spacecraft-Earth angle of the trajectory) and for trajectory correction maneuvers, while the MGA provides increased capability as the Earth-to-Mars distance increases. After separation from the CS, the lander communicates with the DSN via an X-band downlink, and can initiate a UHF return link to an available orbiter. Communications during EDL are beneficial in case of a failure because they help reconstruct and investigate the cause. Transmission of X-band multiple-frequency shift-keying tones through the low-gain antenna is used to indicate the spacecraft state and the completion of the major EDL events. During the primary and extended surface missions, the X-band transponder is supported by either a high-gain antenna (HGA) or the Lander low-gain antenna (LLGA). The LLGA provides near omnidirectional coverage for both command and low-rate telemetry data. The HGA is a steerable, flat-panel, phased array, providing high-rate reception of command and transmission of telemetry data. During the

surface missions, the uplink and downlink rate capability via the HGA depends on the Mars-Earth distance. In addition to the X-band system, the UHF system can be also used for the portion of EDL where the lander is suspended on the bridle. Once on the surface, the UHF system is used to communicate with the AD during its flights and as a backup communications system (in case the X-band link is not available).

7.4. Propulsion subsystem

This function is realized by the so-called Cruise Stage Propulsion System (CSPS), a Helium-pressurized mono-propellant blowdown feed system with hydrazine. The thrusters have been selected among the MONARC series produced by Moog [42]. They are all characterized by a specific impulse close to 230 s. The mass and volume of fuel, pressurizer and tanks have been estimated starting from the total mission ΔV of 108 m/s (accounting for the targeting maneuver, orbit correction impulses, contingencies, an estimate of the attitude control requirements and the due margins) and the dry mass of SMS excluding the propulsion module. The CSPS consists of two spherical fuel tanks, thrusters and miscellaneous components. From *a priori* estimates, an initial guess of 15 kg for the fuel mass is assumed and used to compute the volume of the fuel tanks. The total dry mass of SMS is then re-computed by adding the mass of the CSPS to the initial dry mass without it. The required fuel mass is obtained via Tsiolkovsky rocket equation. This value is used to initialize the procedure again. The iterations are repeated till convergence of the fuel mass. The final value is summed to obtain the wet mass of SMS. Note that apart from the 320 kg restriction due to the performance of Vega, there is also an implicit constraint on the magnitude of the interplanetary maneuvers, mainly due to the thermal stress on the thrusters when firing uninterruptedly for long intervals. This issue has been dealt with by conceiving a combination of eight low-thrust (1 N) actuators distributed in two identical clusters and two high-thrust ($\sim$ 4 N) thrusters: the 1-N actuators shall take care of small orbit correction maneuvers and attitude control, whereas the 4-N thrusters shall execute the large target-

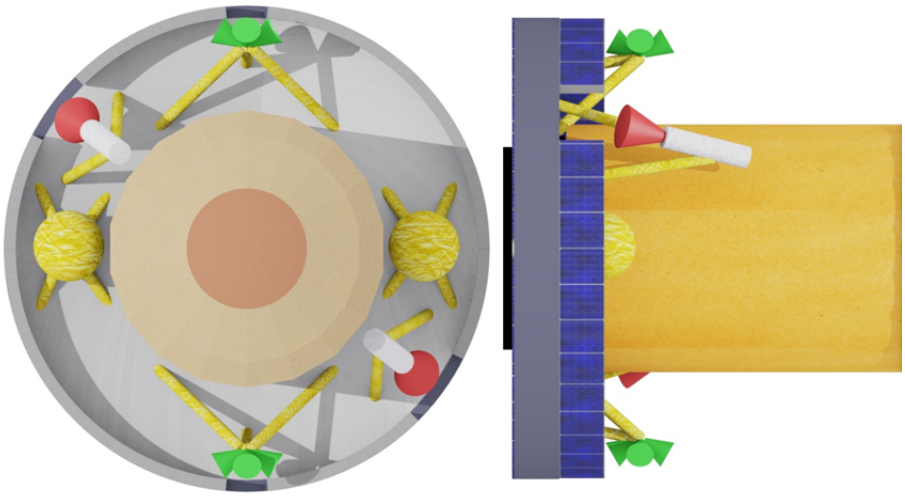

Figure 24: Top and side view of the CSPS: the two spherical tanks (in yellow), the two large thrusters (in white and red) and the two clusters of 1-N actuators (in green). The cylindrical element in the middle is the Lander with the DHS. The side of the CS is partially covered with photovoltaic cells.

ing maneuver at Mars approach. The general layout of the propulsion system is shown in Fig. 24.

8. Conclusions

In this paper we have presented the SMS project, a proposed small European Mars lander. We have provided a comprehensive review of the objectives, the concept and the spacecraft design. We have focused on the most innovative aspects, i.e., the umbrella-like heat shield and the kinematics of the EDL, the two payloads and the way of achieving interplanetary injection with a launcher (Vega) designed for geocentric orbit satellites. All these features make SMS a unique and challenging mission. It is even more so if we consider its small mass and low cost. The latter has been estimated by means of state-of-the-art CER models [43] for small spacecraft on the basis of the sizing parameters of its several components and subsystems and assuming 6-7 years of development. The

scientific and technological objectives are of great interest for the understanding of the mechanisms that drive the Mars climate and in preparation to future Mars exploration missions. In the next step of the development (phase A) we intend to expand the scientific and industrial team, and we shall make a thorough assessment of the adopted solutions, refine the models and iterate through the design.

Acknowledgments

The authors wish to thank the two anonymous referees for their valuable advise. The study here presented has been carried out under ESA Contract No. 4000115306/ 15/NL/LF/as (11/12/2015).

References

[1] W. R. Corliss, The Viking mission to Mars, Tech. rep., Scientific and Technical Information Office, National Aeronautics and Space Administration (1974).

[2] M. P. Golombek, The Mars Pathfinder mission, Journal of Geophysical Research 102 (1997) 3953–3966. doi:10.1029/96JE02805.

[3] J. A. Crisp, M. Adler, J. R. Matijevic, et al., Mars Exploration Rover mission, Journal of Geophysical Research (Planets) 108 (2003) 8061. doi:10.1029/2002JE002038.

[4] P. H. Smith, Phoenix Science Team, The Phoenix Mission to Mars, Vol. 35 of Lunar and Planetary Science Conference, 2004.

[5] J. P. Grotzinger, J. Crisp, A. R. Vasavada, et al., Mars Science Laboratory Mission and Science Investigation, Space Science Reviews 170 (2012) 5–56. doi:10.1007/s11214-012-9892-2.

[6] W. B. Banerdt, S. Smrekar, P. Lognonné, et al., InSight: A Discovery Mission to Explore the Interior of Mars, Vol. 44 of Lunar and Planetary Science Conference, 2013, p. 1915.

[7] O. Witasse, M. Allen, The ESA/NASA ExoMars Trace Gas Orbiter, in: EPSC-DPS Joint Meeting, 2011, p. 109.

[8] Second ExoMars mission moves to next launch opportunity in 2020, http://www.esa.int/Our_Activities/Space_Science/ExoMars (last viewed 6/11/2016) (2016).

[9] R. Savino, R. Aurigemma, P. Dell'Aversana, et al., IRENE Preliminary Study (Italian Re-Entry NacellE Preliminary Study), in: Proceedings of the 10th International Planetary Probe Workshop, 2013.

[10] F. Esposito, The DREAMS experiment on-board the Schiaparelli lander of ExoMars mission, European Planetary Science Congress 10 (2015) EPSC2015–364.

[11] F. Esposito, L. Colangeli, V. Della Corte, et al., MEDUSA: Observation of atmospheric dust and water vapor close to the surface of Mars, International Journal of Mars Science and Exploration 6 (2011) 1–12. doi:10.1555/mars.2011.0001.

[12] L. Colangeli, V. della Corte, F. Esposito, et al., The GIADA experiment for the Rosetta mission, in: L. Colangeli, E. Mazzotta Epifani, P. Palumbo (Eds.), The New Rosetta Targets. Observations, Simulations and Instrument Performances, Vol. 311 of Astrophysics and Space Science Library, 2004, p. 271. doi:10.1007/978-1-4020-2573-0_25.

[13] L. A. Young, E. W. Aiken, V. Gulick, et al., Rotorcraft as Mars Scouts, in: Aerospace Conference Proceedings, IEEE, 2002. doi:10.1109/AERO.2002.1036856.

[14] L. A. Young, R. Chen, E. Aiken, et al., Design Opportunities and Challenges in the Development of Vertical Lift Planetary Aerial Vehicles, in:

Proceedings of the American Helicopter Society International Vertical Lift Aircraft Design Specialist's Meeting, 2000.

[15] L. A. Young, Vertical Lift Not Just for Terrestrial Flight, in: AHS/AIAA/RaeS/SAE International Powered Lift Conference, 2000.

[16] G. Savu, C. Oprisiu, O. Trifu (Eds.), An autonomous flying robot for Mars exploration, 1993.

[17] P. C. O'Brien, Using a Robotic Helicopter to Fuel Interest In and Augment the Human Exploration Of The Planet Mars, in: AIAA Space 2003 Conference and Exposition, AIAA SPACE Forum, 2003, AIAA 2003-6275. doi:10.2514/6.2003-6275.

[18] E. Landau, Helicopter Could Be 'Scout' for Mars Rovers, http://www.jpl.nasa.gov/news/news.php?feature=4457 (last viewed 25/3/2017).

[19] A. Datta, J. Chopra, O. Bao, et al., The Martian Autonomous Rotary-wing Vehicle, Tech. rep., Alfred Gessow Rotorcraft Center, Department of Aerospace Engineering, University of Maryland, College Park, Maryland (2000).

[20] B. Datta, D. Roget, G. Griffiths, et al., Design of a Martian Autonomous Rotary-Wing Vehicle, Journal of Aircraft 40 (3) (2003) 461–472. doi:10.2514/2.3141.

[21] L. A. Young, E. W. Aiken, M. R. Derby, et al., Experimental Investigation and Demonstration of Rotary-Wing Technologies for Flight in the Atmosphere of Mars, in: 58th Annual Forum of the American Helicopter Society, 2002.

[22] J. Savu, O. Trifu, Photovoltaic Rotorcraft for Mars Missions, in: 31st AIAA/ASME/SAE/ASEE Joint Propulsion Conference and Exhibit, 1995.

[23] J. G. Leishman, Principles of Helicopter Aerodynamics, 2nd Edition, Cambridge Aerospace Series, 2006.

[24] New Skysense charging pad enables drones to dock recharge and fly again, http://www.skysense.co/blog/2014/11/charging-pad-drones-dock (last viewed 25/03/2017) (2014).

[25] Point Gray Cameras Catalogue, 2016, https://www.ptgrey.com/ (last viewed 6/11/2016).

[26] A. D. Wu, E. N. Johnson, A. A. Proctor, Vision-Aided Inertial Navigation for Flight Control, in: 2005 AIAA Guidance, Navigation, and Control Conference and Exhibit, 2005, AIAA 2005-5998.

[27] J. Li, Y. Bi, M. Lan, Real-time Simultaneous Localization and Mapping for UAV: a Survey, in: International Micro Air Vehicle Competition and Conference, 2016, pp. 237–242.

[28] E. M. Standish, Keplerian elements for the approximate positions of the major planets, http://ssd.jpl.nasa.gov/txt/aprx_pos_planets.pdf (last viewed 6/11/2016), Solar System Dynamics, JPL/Caltech.

[29] Vega User's Manual, Issue 4 Revision 0 (2014).

[30] ESA-CAS, CAS-ESA Call for Mission Proposals, Technical Annex, Tech. rep., European Space Agency & Chinese Academy of Science (2014).

[31] P. McNamara, The LISA Pathfinder Mission, in: 40th COSPAR Scientific Assembly, Vol. 40 of COSPAR Meeting, 2014.

[32] V. Carandente, Aerothermodynamic and mission analyses of deployable aerobraking Earth re-entry systems, Ph.D. thesis, Department of Industrial Engineering, University of Naples "Federico II", Naples (Italy) (2014).

[33] R. D. Braun, R. M. Manning, Mars Exploration Entry, Descent, and Landing Challenges, Journal of Spacecraft and Rockets 44 (2007) 310–323. doi:10.2514/1.25116.

[34] K. T. Edquist, P. N. Desai, M. Schoenenberger, Aerodynamics for the Mars Phoenix Entry Capsule, Journal of Spacecraft and Rockets 48 (5) (2011) 713–726. doi:10.2514/1.46219.

[35] R. Savino, R. Aurigemma, P. Dell'Aversana, et al., European Sounding Rocket Experiment on Hypersonic Deployable Re-Entry Demonstrator, in: Proceedings of the 8th European Symposium on Aerothermodynamics for Space Vehicles, 2015.

[36] J. Cruz, J. Lingard, Aerodynamic Decelerators for Planetary Exploration: Past, Present and Future, in: Proceedings of the AIAA Guidance, Navigation, and Control Conference, 2006.

[37] Cd-Adapco STAR-CCM+ v10.04 User's Guide (2015).

[38] R. Savino, M. De Stefano Fumo, Aerothermodynamic Study of Ultrahigh-Temperature Ceramic Winglet for Atmospheric Reentry Test, Journal of Thermophysics and Heat Transfer 22 (2008) 669–676. doi:10.2514/1.33296.

[39] D. Paterna, R. Monti, R. Savino, et al., Experimental and numerical investigation on Martian atmosphere entry, AIAA Journal of Spacecraft and Rockets 39 (2) (2001) 227–236.

[40] G. Zuppardi, R. Savino, G. Mongelluzzo, Aero-thermo-dynamic analysis of a low ballistic coefficient deployable capsule in Earth re-entry, Acta Astronautica 127 (2016) 593–602. doi:10.1016/j.actaastro.2016.06.041.

[41] G. A. Bird, Molecular Gas Dynamics and Direct Simulation Monte Carlo, Clarendon Press, Oxford, 1998.

[42] Moog Thrusters Catalogue, 2016, http://www.moog.com/products/thrusters.html (last viewed 6/11/2016).

[43] R. E. A. Kellogg, E. Mahr, M. Lobbia, An analogy-based method for estimating the costs of spacecraft, in: Proceedings of the 2005 IEEE Aerospace Conference, 2005, pp. 4441–4447. doi:10.1109/AERO.2005.1559750.